Proceedings of IMECE'02
2002 ASME International Mechanical Engineering Congress and Exposition
November 17-22, 2002, New Orleans, Louisiana, USA

IMECE2002-32539

MULTI-PHASE FLOW AND CONDENSATION IN PROTON EXCHANGE MEMBRANE FUEL CELLS

John M. Stockie
Department of Mathematics and Statistics
University of New Brunswick
Fredericton, New Brunswick, E3B 5A3
Canada
Email: stockie@unb.ca

ABSTRACT

The porous electrodes in a proton exchange membrane fuel cell are characterized by multi-phase flow, involving liquid water and multispecies gases, that are undergoing both condensation and catalyzed reactions. Careful management of liquid water and heat in the fuel cell system is essential for optimizing performance. The primary focus of this study is thus on condensation and water transport, neither of which have yet been studied in as much detail as other aspects of fuel cell dynamics. We develop a two-dimensional model for multi-phase flow in a porous medium that captures the fundamental transport processes going on in the electrodes. The governing equations are discretized using a finite volume approach, and numerical simulations are performed in order to determine the effect of changing operating conditions on fuel cell performance.

NOMENCLATURE

c specific heat ($erg/g\,^oK$)
C concentration (mol/cm^3)
C_2^{sat} saturated water vapor concentration (mol/cm^3)
C_ℓ concentration of liquid water (mol/cm^3)
D_{jk} binary diffusivity for components j, k (cm^2/s)
$\mathbb{D}$ matrix of Maxwell-Stefan diffusivities (cm^2/s)
$\mathbb{D}^{eff}$ matrix of effective diffusivities (cm^2/s)
h_r heat of reaction (erg/mol)
h_v latent heat of vaporization (erg/mol)
H GDL thickness (cm)
$H_o^{\pm}$ condensation(+)/evaporation(−) rate constants (s^{-1})
i current density (A/cm^2)
$\vec{J}$ diffusive molar flux ($mol/cm^2\,s$)
$\jmath(\beta)$ Leverett J-function (dimensionless)
k_T heat transfer coefficient ($erg/cm^2\,s\,^oK$)
$k_{rel,\cdot}$ relative permeability (dimensionless)
K permeability (cm^2)
L domain width (cm)
L_c channel width (cm)
L_s landing area width (cm)
M molar mass (g/mol)
$\vec{N}$ total molar flux ($mol/cm^2\,s$)
P pressure ($dyne/cm^2$)
r mass transfer coefficient (cm/s)
r_ℓ capillary transfer rate at channel/GDL interface (cm/s)
R universal gas constant ($erg/mol\,^oK$)
T temperature (^oK)
$\vec{U}$ velocity (cm/s)

Greek Letters:

α gas volume fraction (dimensionless)
β water vapor volume fraction (dimensionless)
γ surface tension of water (g/s^2)
Γ condensation rate ($mol/cm^3\,s$)
δ catalyst layer thickness (cm)
ε porosity (dimensionless)
κ thermal conductivity ($erg/cm\,s\,^oK$)
μ viscosity ($g/cm\,s$)

ρ density (g/cm^3)
σ electrical conductivity ($A^2\, s/erg\, cm$)

Subscripts:
j,k species index $= 1,2,3$
g gas
ℓ liquid
s solid

Superscripts:
$\sim$ phase-averaged value
$\bar{}$ constant channel value
c porous channel boundary
m membrane boundary
w solid wall (landing area) boundary
y vertical component of a vector

1 INTRODUCTION

In recent years, the growing worldwide concern over air pollution and dwindling fossil fuel supplies, as well as the ensuing government funding decisions and air quality legislation, have been driving research into the development of non-polluting alternatives to traditional energy sources such as the internal combustion engine. One of the leading contenders among low-emission power generation technologies is the proton exchange membrane (or PEM) fuel cell. In principle, a PEM fuel cell generates electrical current by combining oxygen and hydrogen gas in the presence of a catalyst, generating only water as a byproduct. At the heart of the fuel cell is a polymer membrane (typically made of Nafion®) which is permeable only to protons and hence allows reactant gases to be combined together in a controlled fashion.

The primary challenge in developing a mathematical model for fuel cells is the presence of strong coupling between a wide range of nonlinear physical processes, including multispecies diffusion, flow in porous media, heat transport, condensation, catalyzed reaction chemistry, and ion transport in membranes. A great deal of work has appeared in the past several years on modeling of mass transport in PEM fuel cells, such as [1, 2, 3, 4], while more recent work has focused on including water transport [5, 6] and phase change [5, 7, 8]. However, much of this previous work has emphasized single-phase mass transport and coupling the various fuel cell components together, while relatively little work has been done on detailed modeling of condensation in the GDL, which is essential to determining where and under what conditions liquid water will appear.

This paper extends an earlier model (developed in [9, 10]) for multispecies gas transport occurring under isothermal conditions. Our main purpose here is to generalize the model to include temperature dependence, liquid water motion, and phase change. We then test the predictive power of the model by performing a series of numerical simulations.

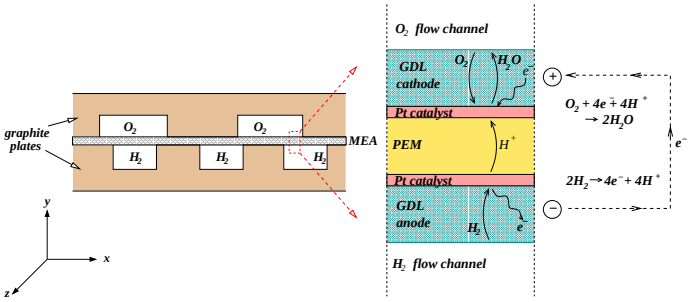

Figure 1. A 2D CROSS-SECTION THROUGH A PEM FUEL CELL.

2 OVERVIEW OF FUEL CELL PHYSICS

A PEM fuel cell consists of a membrane-electrode assembly (or MEA) that is sandwiched between two solid graphite plates, as pictured in a 2D cross-section in Fig. 1. Into the plates are etched flow channels through which the reactant gases are supplied, with oxygen gas on one side and hydrogen on the other. The MEA consists of a polymer membrane, on either side of which is attached an electrode (also known as a gas diffusion layer or GDL) that is composed of a thin layer of carbon fiber paper. The interface between membrane and electrode is where the actual reactions occur, and to this end the interface is impregnated with a platinum catalyst. On the anode side, hydrogen diffuses through the GDL to the catalyst layer where it is dissociated into hydrogen ions and electrons. The protons in turn diffuse across the membrane to the cathode catalyst layer, where they react with the oxygen gas and the electrons from the anode to produce water. Connecting the two electrodes in a circuit allows the electrons to flow and hence generate a usable current.

The performance of a fuel cell is measured by its current density, or current drawn per unit area of catalyst. Because of the highly mobile nature of hydrogen molecules, performance is limited primarily by the effectiveness of ion transport in the membrane and by diffusive transport of oxygen in the cathode. In this study, we do not include the physics of the PEM and hence restrict ourselves to transport occuring in the porous GDL of the cathode. While optimizing performance is clearly a very difficult task owing to the many complex phenomena occuring in fuel cells, the primary issues can be organized under two headings:

1. *water management* – since a high water content is required in the PEM in order to maximize proton conductivity, while liquid water in the electrodes hinders gas transport; and
2. *heat management* – high temperatures or thermal gradients tend to damage the very fragile membrane material, and yet the temperature must be high enough in order to avoid excessive condensation and water build-up in the GDL or flow channels.

The main purpose of this paper is to generate a model that will be able to gauge the effect of changes in electrode characteristics and operating conditions on performance in terms of heat and water management.

3 GOVERNING EQUATIONS

In this section, we only briefly outline the equations of motion governing heat and mass transport in the cathode GDL. The model is based on several major assumptions which we list below:

i. variations along-the-channel are assumed to be slight so that we can consider only a two-dimensional cross-section of the fuel cell, as pictured on the left in Fig. 1. Consequently, all solution quantities are functions of x and y only.
ii. the gas mixture behaves as an ideal gas.
iii. the fuel cell system is at thermal equilibrium so that all phases can be described by a single temperature field.
iv. interspecies diffusion in the gas phase is governed by the Maxwell-Stefan equations, while convective transport within both liquid and gas phases is governed by Darcy's Law.
v. all product water is generated in the gas phase, and condensation or evaporation will occur depending on the local temperature and saturation pressure.
vi. a single electrode is considered in isolation, with the coupling to other fuel cell components (channel, membrane and catalyst) relegated to suitably-chosen boundary conditions.

A more detailed discussion of the assumptions and model development can be found in [10] and [11].

The gas inflow at the cathode is usually taken to be pressurized, humidified air, which consists primarily of three species, numbered $k = (1,2,3) = (O_2, H_2O, N_2)$. If the concentration of each gas species is denoted C_k, then the corresponding densities are $\rho_k = M_k C_k$, where M_k denotes the molar mass. Furthermore, the gas mixture has concentration $C = \sum_k C_k$ and density $\rho = \sum_k \rho_k$. Because both gas and liquid are present together in the porous matrix of the GDL, we need to distinguish between the fraction of the pore volume occupied by gas, which we denote α, and that by liquid, denoted $\beta = 1 - \alpha$ (where β is usually referred to as the "*saturation*"). With these definitions, we can write an equation describing conservation of mass in the gas phase:

$$(\alpha\rho)_t + \nabla \cdot \left(\rho \vec{U}_g\right) = -M_2 \Gamma, \tag{1}$$

where $\vec{U}_g$ is the mass-averaged velocity for the gas and Γ represents the water condensation rate. The velocity is assumed to obey Darcy's Law for flow in porous media

$$\vec{U}_g = -\frac{K k_{rel,g}(\beta)}{\mu_g} \nabla P_g, \tag{2}$$

where P_g and μ_g denote the gas pressure and viscosity, and $K = 10^{-8}\ cm^2$ is the permeability of the GDL. The function $k_{rel,g}$ is a saturation-dependent function called the relative permeability, which is typically taken to be of the form $k_{rel,g}(\beta) = (1-\beta)^3$ (for porous media such as soils and rock). The mixture is assumed to obey the ideal gas law, from which

$$P_g = CRT, \tag{3}$$

with T being the temperature, and R the universal gas constant.

For the condensation rate, we employ a simple relationship developed by Fowler in the context of annular, two-phase flows [12], in which the rate of condensation is taken to be proportional to the degree of water vapor oversaturation, $\Gamma \propto (C_2 - C_2^{sat}(T))$, and C_2^{sat} denotes the saturated vapor concentration, a known function of temperature. Since we expect the saturation to vary significantly under certain operating conditions, the proportionality factor should also depend on on the saturation, and so we assume the following form:

$$\Gamma = \begin{cases} H_o^+ \alpha (C_2 - C_2^{sat}(T)), & \text{if } C_2 \geq C_2^{sat}(T), \\ H_o^- \beta (C_2 - C_2^{sat}(T)), & \text{if } C_2 < C_2^{sat}(T). \end{cases} \tag{4}$$

This form of the condensation rate is similar to that used in both [7] and [5] (except that in the former, they have not included any dependence on saturation). We choose values of the rate constants $H_o^{\pm} = 100\ s^{-1}$, which are similar in magnitude to those reported in [7].

The liquid phase obeys a conservation law similar to that for the gas,

$$\beta_t + \nabla \cdot (\beta \vec{U}_\ell) = \Gamma / C_\ell, \tag{5}$$

where $\vec{U}_\ell$ is the liquid velocity, and the condensation source term is scaled by the (constant) molar concentration of liquid water, C_ℓ. We also assume a Darcy's law relationship for the liquid velocity

$$\vec{U}_\ell = -\frac{K k_{rel,\ell}(\beta)}{\mu_\ell} \nabla P_\ell, \tag{6}$$

where P_ℓ and μ_ℓ are the liquid pressure and viscosity, while $k_{rel,\ell}(\beta) = \beta^3$ is relative permeability for the liquid. The liquid

pressure arises from a combination of gas pressure and capillary pressure [8, 13]

$$P_\ell = P_g + \gamma(\varepsilon/K)^{1/2}\mathcal{J}(\beta), \tag{7}$$

which is a standard empirical relationship used in groundwater flow and oil reservoir simulation. Here, $\varepsilon = 0.74$ is the porosity of the medium, γ is the surface tension for water, and $\mathcal{J}(\beta)$ is the well-known Leverett function which often assumed to take the form $\mathcal{J}(\beta) = 1.417(1-\beta) - 2.120(1-\beta)^2 + 1.263(1-\beta)^3$.

Within the gas mixture, the individual species are affected by both convection and diffusion, and hence obey conservation laws of the form

$$(\alpha C_1)_t + \nabla \cdot \overbrace{\left(C_1\vec{U}_g + \vec{J}_1\right)}^{\vec{N}_1} = 0, \tag{8}$$

$$(\alpha C_2)_t + \nabla \cdot \underbrace{\left(C_2\vec{U}_g + \vec{J}_2\right)}_{\vec{N}_2} = -\Gamma, \tag{9}$$

where $\vec{J}_k$ are the molar diffusive fluxes relative to the mass-averaged velocity, and the total (convective + diffusive) flux is denoted by $\vec{N}_k = C_k\vec{U}_g + \vec{J}_k$. Notice the presence of a sink term due to condensation in Eq. (9) for the water vapor species. The diffusive fluxes are determined by the Maxwell-Stefan equations, which can be written as [14]

$$\begin{bmatrix}\vec{J}_1\\ \vec{J}_2\end{bmatrix} = -C\,\mathbb{D}^{eff}\cdot\begin{bmatrix}\nabla(C_1/C)\\ \nabla(C_2/C)\end{bmatrix}. \tag{10}$$

The Maxwell-Stefan diffusivities form a 2×2 matrix, $\mathbb{D} = \begin{bmatrix}D_{11} & D_{12}\\ D_{21} & D_{22}\end{bmatrix}$, where the entries D_{jk} depend on the the species concentrations and the binary gas diffusivities in a complicated way (see [10] or [14] for details). The matrix $\mathbb{D}^{eff}$ that appears in Eq. (10) contains the *effective diffusivities*, which are related to the entries of $\mathbb{D}$ via a Bruggeman-type correction, $\mathbb{D}^{eff} = (\varepsilon\alpha)^{3/2}\mathbb{D}$, which corrects the coefficients for the pore space actually available for diffusive transport.

One more equation is needed to close the system, which comes from conservation of energy. We assume for simplicity that the fuel cell system is at local thermal equilibrium, so that all three phases (solid, gas and liquid) have time to reach the same temperature T. Then, the energy equation can be written as

$$(\widetilde{\rho c}\,T)_t + \nabla\cdot(\widetilde{\rho c}\,\widetilde{\vec{U}}T - \widetilde{\kappa}\nabla T) = \frac{i^2}{\sigma} + h_v\Gamma, \tag{11}$$

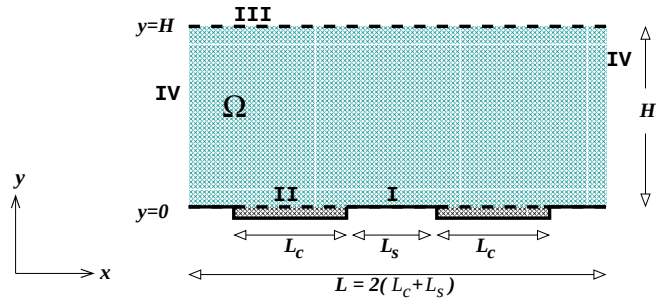

Figure 2. GEOMETRY OF THE MODEL DOMAIN, WITH BOUNDARY COMPONENTS LABELLED I–IV.

where c represents specific heat and κ is thermal conductivity, and the quantities denoted by tildes correspond to parameters that are averaged over all three phases (s =solid, g =gas and ℓ =liquid): $\widetilde{(\cdot)} = (1-\varepsilon)(\cdot)_s + \varepsilon(1-\beta)(\cdot)_g + \varepsilon\beta(\cdot)_\ell$. The two source terms appearing on the right hand side of Eq. (11) arise respectively from from ohmic heating and condensation (where i is the average current density, σ the electrical conductivity, and h_v the latent heat of vaporization).

Equations (1)–(11) together represent a coupled system of five nonlinear partial differential equations to be solved for the unknown quantities ρ, C_1, C_2, β and T, all of which are functions of (x,y,t). We next describe the model geometry and boundary conditions.

3.1 Boundary Conditions

We take a 2D slice through the cathode overlapping with two channels, as pictured in Fig. 2. The channels have a width of L_c, and are separated by a solid graphite "landing area" of width L_s. The length of the domain is then given by $L = 2(L_c + L_s)$, and the thickness of the GDL is denoted by H. The boundary is separated into four regions, each of which is discussed separately below.

I. Solid bottom wall: This part of the boundary along $y = 0$ is impermeable to both gas and liquid and so the following no-flux boundary conditions are applied:

$$J_1^y = J_2^y = N_1^y = 0, \tag{12a}$$

$$\text{and} \qquad \frac{\partial\beta}{\partial y} = 0, \tag{12b}$$

where a superscript y denotes the vertical component of a vector quantity. The solid wall is maintained at a constant temperature of $\overline{T}^w$ (by means of a coolant that is pumped through small channels bored in the graphite plate) and so we impose the following

heat transfer condition, analogous to Newton's law of cooling:

$$\widetilde{\kappa}\frac{\partial T}{\partial y} = k_T^w(T - \overline{T}^w), \tag{12c}$$

where k_T^w is an interfacial heat transfer coefficient with values taken from the literature (e.g., [15]).

II. Porous channel boundary: Across the channel/GDL interface, gases are assumed to diffuse at a rate proportional to the difference in concentrations, so that

$$J_k^y = r_k^c(\overline{C}_k - C_k), \tag{13a}$$

for $k = 1, 2$. Here, r_k^c is a mass transfer coefficient and $\overline{C}_k$ represents the species concentrations in the inlet gas flow. The coefficient r_k^c can be estimated by means of the Sherwood number, $Sh = r_k^c L_d/D$, where D is the diffusivity, L_d is the channel depth, and Sh is obtained from experiments reported in the literature.

We also require that the mixture pressure be continuous across the interface,

$$P_g = \overline{P}_g. \tag{13b}$$

The heat transfer at the porous boundary obeys a similar relationship to that at the solid wall:

$$\widetilde{\kappa}\frac{\partial T}{\partial y} = k_T^c(T - \overline{T}^c), \tag{13c}$$

where k_T^c is a convective heat transfer coefficient and $\overline{T}^c$ is the channel gas temperature. Typical values for k_T^c in fuel cell systems are given in [16].

Finally, the liquid water lying next to the open channel is assumed to be drawn out of the GDL at a speed proportional to the volume fraction of water present,

$$U_\ell^y = -r_\ell \beta, \tag{13d}$$

where r_ℓ is the liquid transfer rate.

III. Membrane/catalyst boundary: If we assume that all oxygen gas which reaches the catalyst layer reacts immediately, then we can take the following flux condition

$$J_1^y = r^m C_1, \tag{14a}$$

which is similar in form to that imposed at the channel/GDL boundary in Eq. (13a). The mass transfer coefficient r^m is chosen so as to obtain a target current density (see [5], for example). If we assume that the reaction produces water in vapor form only, then

$$N_2^y = -2N_1^y \qquad \text{and} \qquad N_3^y = 0. \tag{14b}$$

These flux conditions state that two water molecules are produced for every oxygen molecule in the reaction, and that the PEM boundary is impermeable to gas. The combination of reaction and condensation at this interface leads to a temperature boundary condition of the form

$$\widetilde{\kappa}\frac{\partial T}{\partial y} = h_r N_1^y + h_v \delta\Gamma, \tag{14c}$$

where h_r is the heat of reaction, and the contribution from the heat of condensation has been averaged over the catalyst layer thickness δ. The following boundary condition for the water volume fraction

$$\frac{\partial \beta}{\partial y} = 0, \tag{14d}$$

arises from the assumption that there is no liquid flux into or out of the membrane.

IV. Side walls: On these boundaries, we impose periodic conditions on all solution components.

4 NUMERICAL SIMULATIONS

We next employ a finite volume-based numerical method in order to solver the equations of motion described in the previous section. We only describe the method briefly here, and refer the interested reader to [10] for more details.

The rectangular domain is divided up into a uniform grid, with mesh spacing $h_x = L/n_x$ and $h_y = H/n_y$, where we have chosen $n_x = 32$ and $n_y = 24$. Equations (1)–(11) are discretized in space using a cell-centered, finite volume approach so that the conservation properties of the governing equations are preserved. Second-order centered differences are employed, and because grid points are staggerd one-half mesh spacing from the boundary, satisfying the boundary conditions to second order requires the use of "ghost points," located outside the physical domain. After the system is discretized in space, the resulting system of non-linear ordinary differential equations is integrated in time using the stiff ODE solver, DASSL [17]. In all cases, initial values for the solution components are chosen to be constant, and the

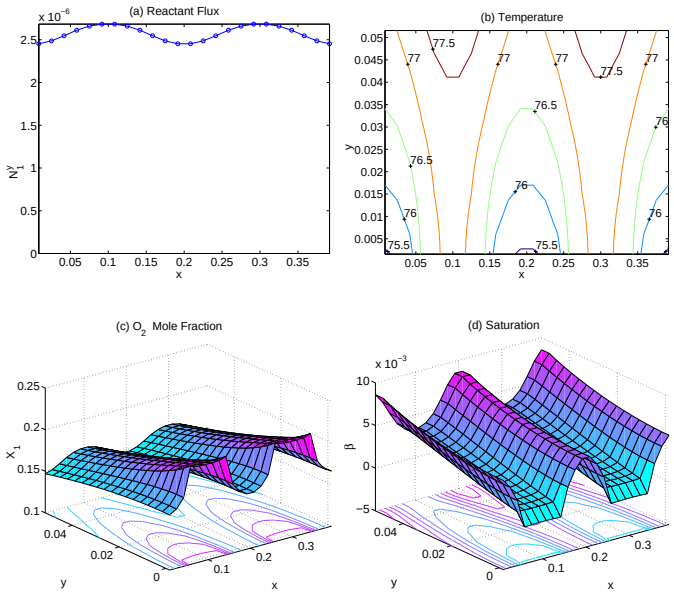

Figure 3. BASE CASE RESULTS.

solution is evolved until a steady state is reached, which usually occurs after approximately 100 s of physical time have elapsed. A typical steady-state computation requires 15 minutes of CPU time on a Dell Precision 620 Workstation with a 733 MHz Pentium Xeon processor.

4.1 The Base Case

We begin with a computations which we refer to as the "base case," corresponding to a cathode running under what can be considered usual operating conditions. The oxygen input stream consists of humidified air at a pressure of $2.0\times10^6\ dyne/cm^2$ (or 2 atm). The parameters corresonding to this simulation are listed in Table 1 (refer to the Nomenclature table for symbol definitions and units of measurement).

The results for the base case are pictured in Fig. 3, which includes plots of the total oxygen flux along the membrane-catalyst layer (N_1^y), temperature (T), oxygen mole fraction (X_1), and water saturation (β). It is clear from the saturation plot that the liquid water remains at very low levels in this situation (below 1%). Indeed in this situation, there is no point within the GDL where the condensation rate is positive. The oxygen mole fraction plots clearly indicate the decrease in reactant from the inlet flow channels (along $y=0$) to the catalyst layer ($y=H$), as well as the "peaks" in reactant concentration that run vertically above the channels. The reactant flux gives an indication of the degree of catalyst utilization and hence also the performance since the O_2 flux is proportional to the current density drawn by the fuel cell. In the base case, the reactant flux is quite uniform across the catalyst layer.

Table 1. PARAMETER VALUES FOR THE "BASE CASE," ALL MEASURED IN CGS UNITS (SEE NOMENCLATURE ON PAGE 1).

Symbol	Value	Symbol	Value
Boundary conditions:		*Material parameters:*	
M_k	$[32.0, 18.0, 28.0]$	ρ_s	0.49
$\overline{X}_k$	$[0.21, 0.10, 0.69]$	ρ_ℓ	1.0
$\overline{T}^c$	74	c_s	1.0×10^7
$\overline{T}^w$	74	c_g	1.0×10^7
$\overline{\rho}$	2.73×10^{-4}	c_ℓ	4.2×10^7
r_k^c	800	κ_s	2.51×10^5
r^m	0.3	κ_g	2.4×10^3
r_ℓ	1.0	κ_ℓ	6.75×10^4
k_T^c	1.5×10^4	μ_g	2.24×10^{-4}
k_T^w	1.1×10^7	μ_ℓ	3.0
$H_o^\pm$	100	C_ℓ	0.0556
Geometrical parameters:		*Other parameters:*	
H	0.05	i	1.0
L_c	0.10	σ	7.273×10^{-5}
L_s	0.10	γ	72.4
L	0.40	h_r	2.72×10^{12}
δ	0.001	h_v	4.54×10^{11}
		K	10^{-8}
		R	8.3145×10^7

4.2 Reducing the Operating Temperature

We next consider the effect of reducing the temperatures $\overline{T}^c$ and $\overline{T}^w$, within the channel mixture and the graphite plate, by 4 degrees to 70^oC. This corresponds, for example, to a lower temperature in the coolant and a correspondingly cooler channel gas mixture. Selected results are displayed in Fig. 4. The temperature has decreased by a degree or two across the GDL, which has led to the onset of condensation. The regions where the gas is oversaturated are shaded in Fig. 4a, from which it is evident that there are pockets of liquid water forming on the catalyst boundary above the solid landing areas and also a small pocket on the lower wall. The actual amount of liquid water present in the GDL can be inferred from the saturation plot, where it is clear that regions near the upper boundary have up to 20% water by volume. The corresponding water velocity is given as a vector plot in Fig. 4c, where the maxiumum value of $|\vec{U}_\ell|$ is approximately $1\times10^{-3}\ cm/s$, which is consistent with the two-phase, isothermal PEM cathode simulations in [8]. Even though there is a significant level of liquid water accumulating near the reaction zone, the change in the reactant flux at the catalyst layer is negligible; hence, we can conclude that at low levels of saturation, the diffusion is not hindered enough to affect the transport of O_2 gas

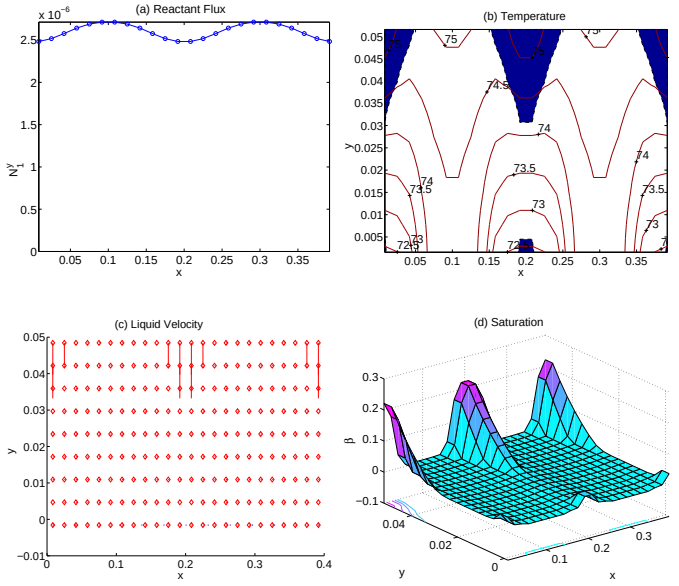

Figure 4. RESULTS WITH CHANNEL AND PLATE TEMPERATURES REDUCED TO 70^oC.

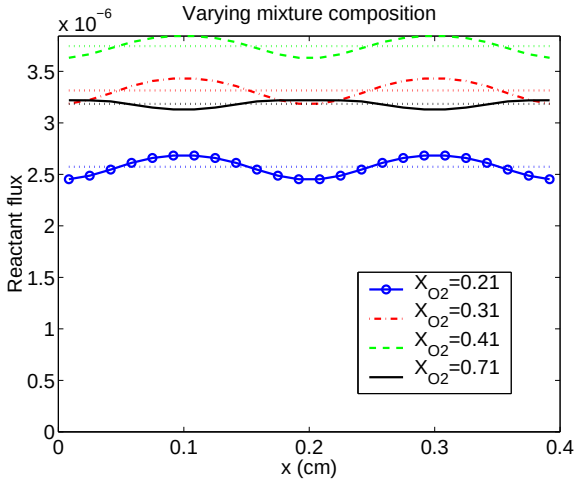

Figure 5. COMPARISON OF REACTANT FLUXES AS O_2 MOLE FRACTION IS INCREASED.

to the reaction zones. However, the presence of liquid water directly adjacent to the catalyst layer is a source for some concern, since there is a potential for flooding of the reaction zones which could have serious impact on performance.

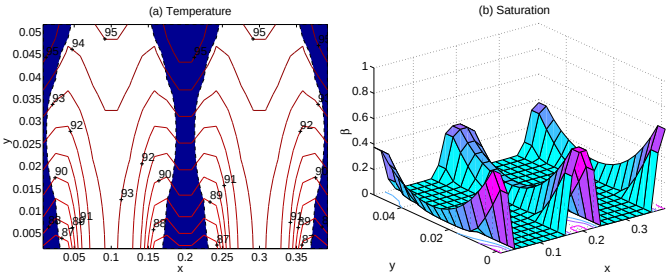

Figure 6. RESULTS WITH CHANNEL O_2 MOLE FRACTION OF 0.71.

4.3 Increasing the Reactant Concentration

While many fuel cells feed the cathode stream with simple pressurized air, there are many situations when purified air having a higher mole fraction of oxygen gas is utilized. To this end, we have varied the mixture composition by taking the channel values of O_2 concentration $X_1 = 0.31, 0.41$ and 0.71, while keeping the saturation constant, $X_2 = 0.10$. The reactant flux profiles are plotted together in Fig. 5, from which we can see that the increased O_2 levels initially enhance performance, with $X_1 = 0.41$ giving the largest average reactant flux at the upper boundary. However, when the channel O_2 concentration is increased further, the reactant flux decreases. The reason for this behavior can be seen in the plots of temperature and saturation in Fig. 6, where the water saturation has risen to such an extent (up to 40% in some locations) that liquid water has led to significant blocking of pores and hence has begun to hinder diffusive transport of oxygen across the GDL. In particular, there is a large portion of the catalyst layer that is bordered by pores containing more than 20% water by volume, which impacts directly on the reaction rate.

5 CONCLUSIONS

We have developed a model for motion of multiphase, flow and condensation within the porous cathode of a proton exchange membrane fuel cell, which is one of the first attempts to model nonisothermal flow including condensation. The model has proven very useful in determining the effect of changes in operating conditions on performance in terms of the transport of oxygen to the reactive catalyst layer. In particular, we have been able to identify regions where condensation is most likely to occur, and also parameter regimes where the presence of liquid water begins to impact on performance.

These results are somewhat limited in their application, due the fact that coupling with other fuel cell components is ignored, and so more work is required in the direction of including the physics of the membrane, catalyst layer, and flow channels. Because water management is so essential in understanding fuel cell performance, this model has great potential for accurate studies of transport phenomena in fuel cells.

ACKNOWLEDGMENT

I would like to thank Keith Promislow and Brian Wetton for many helpful discussions. This research was supported by an operating grant from Natural Sciences and Engineering Research Council of Canada as well as a research grant from the MITACS National Centre of Excellence.

REFERENCES

[1] Gurau, V., Liu, H., and Kakaç, S., 1998, "Two-dimensional model for proton exchange membrane fuel cells," *AIChE Journal*, **44**(11), pp. 2410–2422.

[2] Singh, D., Lu, D. M., and Djilali, N., 1999, "A two-dimensional analysis of mass transport in proton exchange membrane fuel cells," *International Journal of Engineering Science*, **37**(4), pp. 431–452.

[3] Yi, J. S., and Nguyen, T. V., 1999, "Multicomponent transport in porous electrodes of proton exchange membrane fuel cells using the interdigitated gas distributors," *Journal of the Electrochemical Society*, **146**(1), pp. 38–45.

[4] Thampan, T., Malhotra, S., Zhang, J., and Datta, R., 2001, "PEM fuel cell as a membrane reactor," *Catalysis Today*, **67**, pp. 15–32.

[5] He, W., Yi, J. S., and Nguyen, T. V., 2000, "Two-phase flow model of the cathode of PEM fuel cells using interdigitated flow fields," *AIChE Journal*, **46**(10), pp. 2053–2064.

[6] Hsing, I.-M., and Futerko, P., 2000, "Two-dimensional simulation of water transport in polymer electrolyte fuel cells," *Chemical Engineering Science*, **55**, pp. 4209–4218.

[7] Rowe, A., and Li, X., 2001, "Mathematical modeling of proton exchange membrane fuel cells," *Journal of Power Sources*, **102**, pp. 82–96.

[8] Wang, Z. H., Wang, C. Y., and Chen, K. S., 2001, "Two-phase flow and transport in the air cathode of proton exchange membrane fuel cells," *Journal of Power Sources*, **94**(1), pp. 40–50.

[9] Promislow, K., and Stockie, J. M., 2001, "Adiabatic relaxation of convective-diffusive gas transport in a porous fuel cell electrode," *SIAM Journal on Applied Mathematics*, **62**(1), pp. 180–205.

[10] Stockie, J. M., Promislow, K., and Wetton, B. R., 2001, "A finite volume method for multicomponent gas transport in a porous fuel cell electrode," Submitted to *International Journal for Numerical Methods in Fluids*.

[11] Stockie, J. M. Promislow, K., and Wetton, B. R., 2002, "A model for multicomponent, condensing gas mixtures in hydrophobic porous media," In preparation.

[12] Fowler, A. C., 1997, *Mathematical Models in the Applied Sciences*, Cambridge University Press, Cambridge.

[13] Udell, K. S., 1983, "Heat transfer in porous media heated from above with evaporation, condensation, and capillary effects," *Journal of Heat Transfer*, **105**, pp. 485–492.

[14] Taylor, R., and Krishna, R., 1993, *Multicomponent Mass Transfer*, John Wiley and Sons, New York.

[15] Bradean, R. P., Promislow, K., and Wetton, B. R., 2001, Heat and mass transfer in porous fuel cell electrodes. In *Proceedings of the International Symposium on Advances in Computational Heat Transfer*, Queensland, Australia.

[16] Amphlett, J. C., Mann, R. F., Peppley, B. A., Roberge, P. R., and Rodrigues A., 1996, A model predicting transient responses of proton exchange membrane fuel cells *Journal of Power Sources*, **61**, pp. 183–188.

[17] Petzold, L. R., 1982, *A Description of DASSL: A Differential/Algebraic System Solver*, Technical Report #SAND82–8637, Sandia National Laboratories, Livermore, CA.